Chalcogenide-Bound Erbium Complexes: Paradigm Molecules for Infrared Fluorescence Emission

G. A. Kumar and Richard E. Riman*

Department of Ceramic & Material Engineering, The State University of New Jersey, 607 Taylor Road, Piscataway, New Jersey 08854-8065

L. A. Diaz Torres and O. Barbosa Garcia

Centro de Investigaciones en Optica, Leon Gto., Mexico City 37150, Mexico

Santanu Banerjee, Anna Kornienko, and John G. Brennan

Department of Chemistry and Chemical Biology, Rutgers, The State University of New Jersey, 607 Taylor Road, Piscataway, New Jersey 08854-8087

Received April 11, 2005. Revised Manuscript Received June 23, 2005

The near-infrared luminescence properties of the nanoscale erbium ceramic cluster $(THF)_{14}Er_{10}S_6Se_{12}I_6$ (Er10, where THF = tetrahydrofuran) and the molecular erbium thiolate $(DME)_2Er(SC_6F_5)_3$ (Er1, where DME = 1,2-dimethoxyethane) were studied by optical absorption, photoluminescence, and vibrational spectroscopy. The calculated radiative decay time of 4 ms for the $^4I_{13/2} \rightarrow {}^4I_{15/2}$ transition is comparable to the reported values for previously reported organic complexes. The recorded emission spectrum of the $^4I_{13/2} \rightarrow {}^4I_{15/2}$ transition was centered at 1544 nm with a bandwidth of 61 and 104 nm for Er10 and Er1, respectively, with stimulated emission cross sections of 1.3×10^{-20} cm^2 (Er10) and 0.8×10^{-20} cm^2 (Er1) that are comparable to those of solid-state inorganic systems. Lifetime measurements of the 1544 nm decay showed a fluorescence decay time of the order of 3 ms for Er10 that, together with the radiative decay time, yielded a quantum efficiency above 78%, which is considered to be the highest reported value for a "molecular" erbium compound. This efficiency is attributed to the absence of direct Er coordination with fluorescence quenching vibrational groups such as hydrocarbon and bonding of hydroxide groups. The direct coordination of S, Se, and I accounts for the improved fluorescence spectral properties. These properties result because these anions are heavy and form stable but weak bonds to facilitate a low phonon energy host environment for the erbium.

Introduction

Nanomaterials currently captivate the materials world with the promise of exciting applications in science and technology. The dramatic improvements of the various physical, electronic, and chemical properties in the nano-regime presage the application of these materials in the fabrication of optical, electronic, and biological devices.

Erbium (Er)-doped materials have attracted considerable attention because of their potential applications in optoelectronics.[1,2] The 1.5 μm emission arising out of the $^4I_{13/2} \rightarrow {}^4I_{15/2}$ transition in the trivalent state of erbium (Er^{3+}) is technologically important in the telecommunication area because of the low attenuation of this energy by silica-based fiber optics. There exists a plethora of spectroscopic studies examining the infrared emission of Er^{3+} in various hosts, including both crystalline and amorphous materials,[3−5] that have led to the development of active optical devices including lasers and fiber or planar waveguides. The performance of Er^{3+}-based optical devices depends on a range of important materials properties, i.e., fluorescence lifetime, stimulated emission cross section, effective bandwidth of the emission band (1.5 μm), and the Er^{3+} concentration. Of these, the measured fluorescence lifetime of the 1.5 μm emission band ultimately determines the quantum efficiency of the material.

Organic complexes of erbium have been examined as an inexpensive and simple means to make optical devices. Unfortunately, these complexes have a lifetime of the $^4I_{13/2}$ excited state in the microsecond regime, resulting in low quantum efficiency.[6−10] These low quantum efficiencies are associated with the high-frequency CH/OH vibrational bands

* Corresponding author. E mail: riman@rci.rutgers.edu.

(1) Desurvire, E. *Sci. Am.* **1992**, *266*, 96.
(2) Glass, A. M. *Phys. Today* **1993**, *46*, 34.
(3) Kaminskii, A. A. *Laser crystals their physics and properties*; Springer-Verlag: New York, 1981.
(4) Becker, P. C.; Olsson, N. A.; Simpson, J. R. *Erbium doped fiber amplifiers-Fundamental and technology*; Academic Press: New York, 1999.
(5) Reisfeld, R.; Jorgensen, C. K. *Lasers and excited states of Rare earths*; Springer-Verlag: New York, 1977.
(6) Hebbink, G. A.; Reinboudt, D. N.; van Veggel, F. C. J. M. *Eur. J. Org. Chem.* **2001**, 4101.
(7) Sloof, L. H.; Polman, A. *J. Appl. Phys.* **1998**, *83*, 497.
(8) Wolbers, M. P. O.; van Veggel, F. C. J. M.; Snellink-Ruel, B. H. M.; Hofstraat, J. W.; Geurts, F. A. J.; Reinhoudt, D. N. *J. Am. Chem. Soc.* **1997**, *119*, 138.

10.1021/cm050770f CCC: $30.25
Published on Web 09/09/2005

of the organic ligands that couple with the Er^{3+}, resultantly reducing the lifetime of the emitting level by multiphonon relaxation.

Lifetimes are considerably longer in solid-state materials, where low phonon energy hosts for the rare earth greatly diminish multiphonon relaxation.[11] Crystalline and amorphous materials have excited-state Er lifetimes in the microsecond regime, and quantum efficiencies range from 50 to 100%.[3] Unfortunately, the processing of solid-state Ln materials for optical applications such as telecommunications presents a range of challenges, depending on the types of materials pursued. Amorphous glasses are difficult to supercool and have poor Ln solubility.[12] Single crystals that offer excellent solubility can be chosen but they are difficult to grow in large sizes and cost effectively.[13−15] More recently, we proposed the concept of synthesizing and dispersing nanocrystals of Ln-soluble hosts in a variety of matrixes, which can be organic or inorganic.[16−20] However, while this novel use of nanotechnology offers a low-cost approach to making transparent Ln-based materials, deagglomeration and colloidal stabilization methods are required to maintain particles sufficiently below 100 nm to maintain low scattering losses. The challenge for accomplishing this on a manufacturing scale because of the limited methods to make and disperse nanoparticles focuses us on reconsidering the molecular approaches. Molecular compounds can thermodynamically dissolve in solutions while nanoparticles can only be kinetically stabilized. Molecular compounds can be produced with conventional manufacturing methods while nanoparticle manufacturing methods are not currently well defined.

The incorporation of molecular Ln compounds requires that we overcome this issue concerning low quantum efficiency. To that end, we have conceived of paradigm molecular structures that offer a Ln environment characteristic of a low phonon energy host. Such a structure has the Ln coordinated or bound by low phonon energy ligands, such as halide or chalcogenides in the form of a ceramic cluster or fragment. Hydrocarbon and hydroxyl species can exist in the complex provided they do not directly participate in the nearest neighbor coordination sphere encapsulating Ln. Such species are envisioned to shroud the cluster in the second coordination sphere or greater. By assuming such a configuration, solubility in organic media such as liquids and polymers is feasible, which yield excellent transmission characteristics because there is no second phase to scatter light.

In this paper, we report for the first time optical studies that assess the fluorescence emission characteristics of the paradigm molecular complexes $(THF)_{14}Er_{10}S_6Se_{12}I_6$ (Er10, where THF = tetrahydrofuran)[21] and $(DME)_2Er(SC_6F_5)_3$ (Er1, where DME = 1,2-dimethoxyethane).[22] These Er compounds were chosen to establish whether or not encapsulation of the emitting Er with chalcogenides and fluorocarbon ligands could effectively reduce nonradiative vibrational loss.

Experimental Section

General Methods. All syntheses were carried out under ultrapure nitrogen (WELCO CGI, Pine Brook, NJ), using conventional drybox or Schlenk techniques. Solvents (Fisher Scientific, Agawam, MA) were refluxed continuously over molten alkali metals or K/benzophenone and collected immediately prior to use or purified with a dual-column Solv-Tek solvent purification system (Solv-Tek, Inc., Berryville, VA). Er and Hg were purchased from Strem Chemicals (Newburyport, MA). HSC_6F_5 was purchased from Aldrich. Anhydrous pyridine (Aldrich Chemicals, Milwaukee, WI) was purchased and refluxed over KOH (Aldrich). $(THF)_{14}Er_{10}S_6Se_{12}I_6$ was prepared according to the literature procedure[21] while $(DME)_2Er(SC_6F_5)_3$ was prepared with a modified version of the literature preparation,[22] as follows.

Synthesis of $(DME)_2Er(SC_6F_5)_3$. Er (0.171 g, 1.02 mmol) and $Hg(SC_6F_5)_2$ (0.961 g, 1.61 mmol) were combined in DME (ca. 30 mL), and the mixture was stirred at room temperature until all the Er dissolved and shiny metallic Hg (0.31 g, 96%) was collected at the bottom of the flask. The resultant light pink colored solution was filtered away under dry nitrogen, reduced in volume to ~20 mL, and layered with 10 mL of hexane to give pink crystals (0.876 g, 93%) that were identified by melting point (215 °C), compared with the published IR spectra,[22] and had their unit cell determined with X-ray diffraction.

Spectroscopy. Absorption measurements were carried out with crystalline powder dissolved in THF using a double beam spectrophotometer (Perkin-Elmer Lambda 9**,** Wellesley, MA) in a 1 cm cuvette using THF as the reference solvent. The emission spectra of the powdered samples were recorded by exciting the sample with a 980 nm band of a laser diode in the 90°-excitation geometry. The diode current was kept at 960 mA throughout the experiment to maintain the same excitation laser power. The emission from the sample was focused onto a 1 m monochromator (Jobin Yvon, Triax 550, Edison, NJ) and detected by a thermoelectrically cooled InGaAs detector. The signal was intensified with a lock-in amplifier (SR 850 DSP, Stanford Research System, Sunnyvale, CA) and processed with a computer controlled by Spectramax commercial software (GRAMS 32, Galactic Corp., Salem, NH). To measure the decay time, the laser beam was modulated at 32 Hz by a chopper and the signal was collected on a digital oscilloscope (model 54520A, 500 MHz, Hewlett-Packard**,** Palo Alto, CA).

Data Analysis. The radiative lifetime (τ_{RAD}) of the infrared emitting state is related to the total spontaneous emission probability

(9) Wolbers, M. P. O.; van Veggel, F. C. J. M.; Peters, F. G. A.; van Beelen, E. S.; Hofstraat, J. W.; Geurts, F. A. J.; Reinhoudt, D. N. *Chem.—Eur. J.* **1998**, *4*, 772.
(10) Hasegawa, Y.; Okhubo, T.; Sogabe, K.; Kawamura, Y.; Wada, Y.; Nakashima, N.; Yanagida, S. *Angew. Chem., Int. Ed.* **2000**, *39*, 357.
(11) Soga, K.; Wang, W.; Riman, R. E.; Brown, J. B.; Mikeska, K. R. *J. Appl. Phys.* **2003**, *93*, 2946.
(12) Almeida, R. M. *Halide glasses for Infrared Fiberoptics*; NATO ASI Series; Kluwer Academic Publishers: Norwell, MA; 1986.
(13) Krupke, W. F. *Phy. Rev. B.* **1966**, *145*, 325.
(14) Carnall, W. T.; Goodman, G. L.; Rajnak, K.; Rana, R. S. *J. Chem. Phys.* **1989**, *90*, 3443.
(15) Weber, M. J. *Phys. Rev.* **1967**, *157*, 262.
(16) Ballato, J.; Riman, R. E.; Snitzer, E. *Opt. Lett.* **1997**, *22*, 691.
(17) Kumar, G. A.; Riman, R. E.; Snitzer, E.; Ballato, J. *J. Appl. Phys.* **2004**, *95*, 40.
(18) Kumar, G. A.; Chae, S. C.; Jang, Y. N.; Bae, I. K.; Riman, R. E.; Moon, H. S. *J. Appl. Phys.* **2004**, *95*, 3243.
(19) Riman, R. E.; Ballato, J. Rare Earth Doped Host Materials. U.S. Patent 6,699,406, March 2, 2004.
(20) Riman, R. E.; Ballato, J. Optically Transparent Nanocomposite Materials. Continuation-in-part U.S. Patent Application, filed March 2, 2004.
(21) Kornienko, A.; Emge, T. J.; Kumar, G. A.; Riman, R. E.; Brennan, J. G. *J. Am. Chem. Soc.* **2005**, *127*, 3501.
(22) Melman, J.; Rhode, C.; Emge, T. J.; Brennan, J. G. *Inorg. Chem.* **2002**, *41*, 28.

of all the transitions from an excited state by $\tau_{RAD} = (\sum A_{J'J})^{-1}$ where A is calculated using Judd−Ofelt theory[23,24] as

$$A_{rad}(i \rightarrow j) = \frac{64\pi^4}{3h(2J+1)e^2\lambda^3}\left[\frac{n(n^2+2)^2}{9}\right]\sum_{i=2,4,6}\Omega_i\langle^4I_{13/2}||U^i||^4I_{15/2}\rangle^2 \quad (1)$$

where n is the refractive index, Ω_i are the Judd−Ofelt intensity parameters, and $||U^i||$ are doubly reduced matrix elements operators corresponding to the $J \rightarrow J'$ transition. The three Judd−Ofelt parameters were obtained by fitting the measured oscillator strength to the theoretical oscillator strength using the least squares technique. The quality of the fit is determined by the root mean square (RMS) deviation between the experimental and the theoretical values of the dipole strength were obtained from the expression

$$\mathrm{RMS} = [(\sum \Delta S)^2/(N-m)]^{1/2} \quad (2)$$

where ΔS is the difference between the experimental and the calculated dipole strengths, N is the number of transitions, and m is the number of fitting parameters.

The stimulated emission cross section of the 1544 nm band is obtained with the Fuchtbauer−Ladenburg equation,[3]

$$\sigma_{em} = \frac{\lambda^4 A}{8\pi c n^2 \Delta\lambda_{eff}} \quad (3)$$

where $\Delta\lambda_{eff}$ is the effective line width of the emission band obtained by integrating over the entire emission band and dividing by the peak fluorescence intensity.

The lifetime of the emission band is extracted from the decay curve by fitting with the following equation in Monte Carlo (MC) energy transfer model,[25]

$$I_i(t) = \exp\left(-\frac{t}{\tau}\right)\prod_{j=1}^{N_A}\exp[-W_{DA}(R_i - R_j)t] \quad (4)$$

where W_{DA} is the donor to acceptor energy transfer rate separated by the distance R_{ij} ($R_i - R_j$). The major contribution of W_{DA} is from multipolar (W_{MP}), exchange (W_{EX}), or a combination of both (i.e., $W_{DA} = W_{MP} + WEX$). The multipolar interaction rate is obtained from the well-know Forster−Dexter model as follows,[26,27]

$$W_{MP}(R_{ij}) = \left(\frac{C_{DA}}{R_{ij}}\right)^6 + \left(\frac{C_{DA}}{R_{ij}}\right)^8 + \left(\frac{C_{DA}}{R_{ij}}\right)^{10} \quad (5)$$

$$C^s_{DA} = \frac{R_0^s}{\tau_{0D}}$$

where R_0 is the critical donor−acceptor separation and τ_{0D} is the decay time of the donor emission in the absence of energy transfer (lowest concentration limit). For the dipole−dipole interaction the critical separation R_0^6 is given by the expression,[26,27]

$$R_0^{\,6} = \frac{3h^4c^4}{4\pi n^4}Q_A\int\frac{f_S(E)\,f_A(E)\,dE}{E^4} \quad (6)$$

where $f_S(E)$ and $f_A(E)$ are the normalized line shape functions of the sensitizer emission and acceptor absorption spectra, n is the refractive index of the material, Q_A is the oscillator strength of the absorption band of the acceptor that is in resonance with the sensitizer emission transition, and E is the average energy of the overlapping transition.

The exchange interaction is evaluated as follows,

$$W_{EX} = \frac{1}{\tau_{0D}}\exp\left[\gamma\left(1 - \frac{R_{ij}}{R_0}\right)\right] \quad (7)$$

where $\gamma = 2R_0/L$; R_0 is the penetration depth of the exchange interaction, and L is the effective Bohr radius.

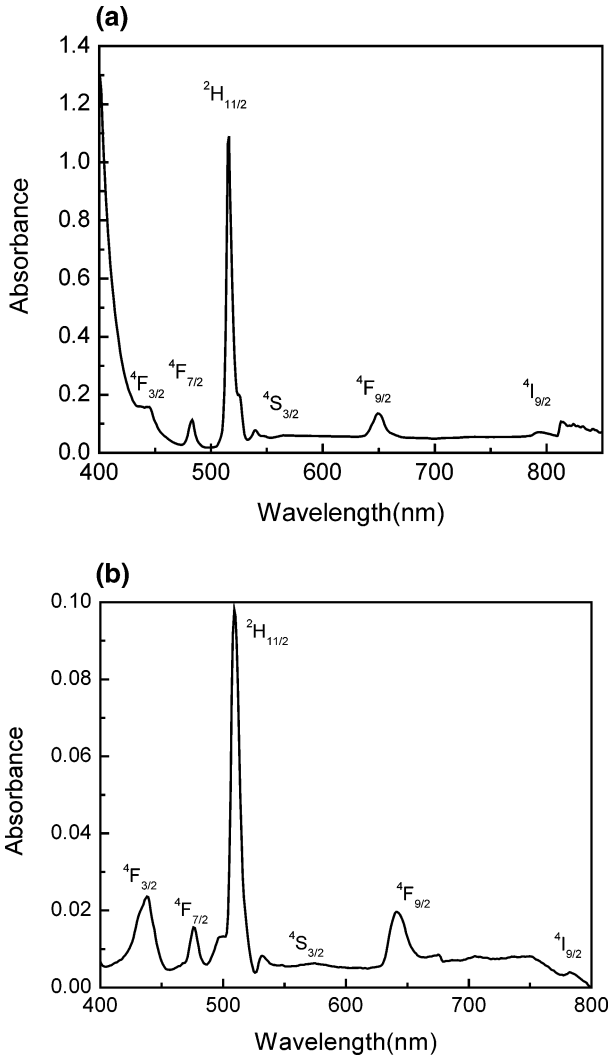

Figure 1. Absorption spectra of (a) $(THF)_{14}Er_{10}S_6Se_{12}I_6$ and (b) $(DME)_2$-$Er(SC_6F_5)_3$.

Results and Discussion

The room-temperature absorption spectra for Er10 and Er1 are shown in Figure 1. Below 400 nm the absorption bands of Er^{3+} ions are overlapped by the onset of the ligand absorption edge ($h\nu = 3$ eV). In the 400−1600 nm region, various f → f absorption bands of Er^{3+} are observed, where the strongest is in the 516 nm region. These bands originate from the $^4I_{15/2}$ ground state of Er^{3+} and the standard notations identify the different transitions. All the observed absorption bands are numerically integrated to obtain the experimental line strength, and the values obtained are summarized in Table 1 along with the observed band positions and their spectral assignments. These values are comparable to those

(23) Judd, B. R. *Phys. Rev. B* **1962**, *127*, 750.
(24) Ofelt, G. S. *J. Chem. Phys.* **1962**, *37*, 511.
(25) Barbosa Garcia, O.; Struck, C. W. *J. Chem. Phys.* **1994**, *100*, 4554.
(26) Forster, T. *Ann. Phys.* **1948**, *2*, 55.
(27) Dexter, D. L. J. *Chem. Phys.* **1953**, *21*, 836.

Table 1. Experimentally Observed Band Positions, Their Spectral Assignments, and Experimental and Computed Absorption Band Line Strengths in (a) $(THF)_{14}Er_{10}S_6Se_{12}I_6$ and (b) $(DME)_2Er(SC_6F_5)_3$

transition from $^4I_{15/2}$ to	transition energy (cm^{-1})	integrated absorption (10^{-7})	S_{meas}[a] (10^{-20} cm^2)	S_{cal}[b] (10^{-20} cm^2)
		(a) $(THF)_{14}Er_{10}S_6Se_{12}I_6$[c]		
$^4F_{7/2}$	483	7.8	2.39	2.61
$^2H_{11/2}$	515	26.34	7.56	7.51
$^4S_{3/2}$	539	6.9	0.89	0.81
$^4F_{9/2}$	649	11.95	2.73	2.77
$^4I_{9/2}$	800	5.25	0.47	0.38
$^4I_{11/2}$	976	10.65	1.62	1.71
$^4I_{13/2}$	1527	59.0	5.72	5.70
		(b) $(DME)_2Er(SC_6F_5)_3$[d]		
$^2K_{15/2}$	367	15.0	2.70	2.50
$^4G_{11/2}$	383	8.9	1.60	1.80
$^4F_{3/2}$	438	10.82	1.78	1.76
$^4F_{7/2}$	476	4.28	2.68	2.50
$^2H_{11/2}$	509	19.59	8.01	7.80
$^4S_{3/2}$	531	1.82	2.0	2.11
$^4F_{9/2}$	641	8.36	2.56	2.60
$^4I_{9/2}$	790	3.20	1.0	0.90

[a] Measured electric dipole line strength. [b] Calculated electric dipole line strength. [c] $\Omega_2 = 8.9 \times 10^{-20}$ cm^2, $\Omega_4 = 2.0 \times 10^{-20}$ cm^2, $\Omega_6 = 3.7 \times 10^{-20}$ cm^2, $\Delta S_{rms} = 0.61 \times 10^{-20}$ cm^2. [d] $\Omega_2 = 8.7 \times 10^{-20}$ cm^2, $\Omega_4 = 2.0 \times 10^{-20}$ cm^2, $\Omega_6 = 3.9 \times 10^{-20}$ cm^2, $\Delta S_{rms} = 0.19 \times 10^{-20}$ cm^2.

of Er^{3+} in many reported inorganic materials.[28−30] The measured line strengths are fitted with the theoretical line strength[23,24] to obtain the three phenomenological intensity parameters. For Er10 these are $\Omega_2 = 8.9 \times 10^{-20}$ cm^2, $\Omega_4 = 2.08 \times 10^{-20}$ cm^2, and $\Omega_6 = 3.75 \times 10^{-20}$ cm^2. For Er1, the corresponding values are $\Omega_2 = 8.7 \times 10^{-20}$ cm^2, $\Omega_4 = 2.0 \times 10^{-20}$ cm^2, and $\Omega_6 = 3.9 \times 10^{-20}$ cm^2, respectively. The RMS values were found to be of the order of $0.19-0.16 \times 10^{-20}$ cm^2, which showed that the Judd−Ofelt model was suitable in predicting the radiative spectral properties with three fitting parameters. The calculated intensity parameters are used to evaluate the transition probability and radiative decay time for the infrared band of interest.

Because the $^4I_{13/2} \rightarrow {}^4I_{15/2}$ transition is responsible for the observed 1544 nm emission (Figure 2), the radiative decay time is required for evaluating the quantum efficiency. The calculated radiative decay time of 3.85 ms is in excellent agreement with the reported value of 4 ms in Er organic complexes.[7] To measure the quantum efficiency, the fluorescence decay time (τ_{fl}) was extracted from the measured decay curve shown in Figure 3. For Er10 the decay curve was fitted with the MC model described in eqs 3−5 to yield a decay time of 3 ms. The fitting was done taking into account all of the cooperative energy transfer processes between the 10 Er atoms located in the various crystallographic sites. Because there is only one Er atom in the Er1 cluster, the MC method is not applicable. The decay time was obtained by an exponential curve fit using the nonlinear curve fitting option using Origin 7 (OriginLab Corporation, Northampton, MA) software which showed a decay time of 2.88 ms. The experimental decay time, together with the calculated radiative decay time, resulted in calculated quantum efficiencies of 78 and 75% for Er10 and E1, respectively. These values are the highest reported efficiencies for molecular compounds. The 1544 nm emission decay time for all reported organic complexes are in the microsecond regime, leading to low reported quantum efficiencies, which range from 0.1 to 0.01%.[6−10] The reported millisecond emission lifetime is typical of a low phonon energy host, which is supported by Table 2 where the emission lifetimes of various classes of low phonon energy hosts are summarized and found to range from 2.3 to 30 ms. More specifically, Er ions encapsulated by selenide, sufide, or iodide have lifetimes that range from 2.3 to 4 ms.[4,29,30]

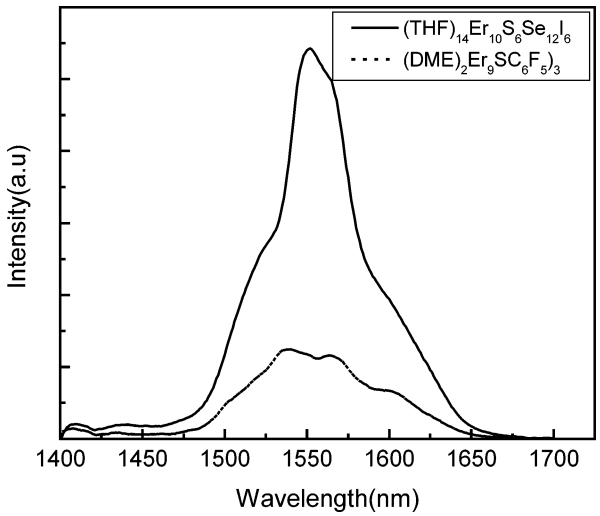

Figure 2. Emission spectra for $(THF)_{14}Er_{10}S_6Se_{12}I_6$ and $(DME)_2Er(SC_6F_5)_3$.

Before analyzing emission cross sections, it is important to survey the structural features associated with Er1 and Er10. ORTEP diagrams of the molecular structures of Er10 and Er1 are shown in Figure 4a,b, respectively. The Er10 compound is composed of an internal, distorted Er_6S_6 double cubane cluster. This internal core is capped to either side with two pairs of $Er_2(SeSe)_3$ moieties, such that the two central Er atoms in the Er_6 framework are encapsulated with chalcogens (4S, 4Se). The remaining eight Er atoms are coordinated to Se, S, O, and I atoms in a monoclinic system with a *C*2/*c* space group. The shortest and longest separations between two Er atoms within an individual cluster are estimated to be 0.39 and 1.025 nm, respectively. The Er^{3+} ionic concentration in the unit cell is 3.5×10^{20} ions/cm^3, which is a high value relative to rare-earth-doped materials with typical values in the $10^{18}-10^{19}$ ions/cm^3 range.

In contrast to Er10, Er1 has three terminal thiolate ligands, two DME molecules, and a dative interaction between Er and an ortho-fluoride that give an eight-coordinate structure.[22] This molecule also crystallized in the *C*2/*c* space group with a lower Er^{3+} ionic unit cell concentration of 1.26×10^{18} ions/cm^3. There are 16 Er−Er separations with distances less than 1.5 nm, with the three shortest separations being 0.82, 0.84, and 0.95 nm.[22]

A comparison of the emission spectra of Er10 and Er1 crystals is shown in Figure 2. Er1 shows an effective bandwidth of 104 nm whereas that of Er10 is 76 nm. The difference in the spectral bandwidth is the result of the

(28) Sardar, D. K.; Gruber, J. B.; Zandi, B.; Huchinson, J. A. Trussell, C. W. *J. Appl. Phys.* **2003**, *93*, 2041.
(29) Fick, J.; Knystautas. E. J.; Villeneuve, A.; Schiettekatte, A.; Roorda, S.; Richardson, K. A. *J. Non-Cryst. Solids* **2000**, *272*, 200.
(30) Ye, C. C.; Hewak, D. W.; Hempstead, M.; Samson, M.; Payne, D. N, *J. Non-Cryst. Solids* **1996**, *208*, 56.

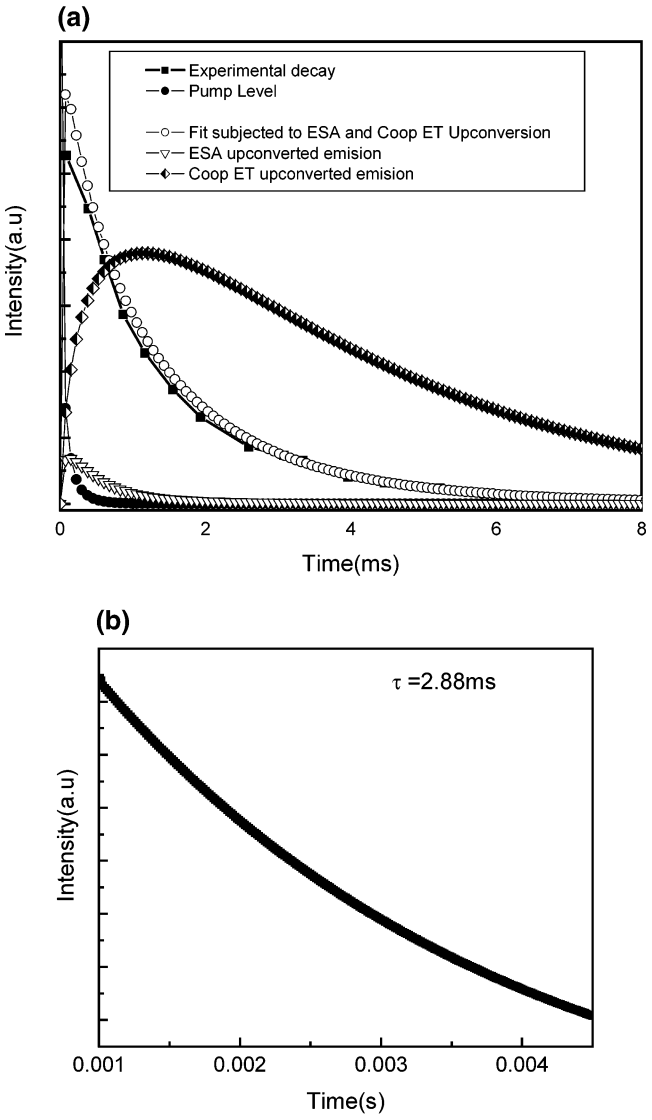

Figure 3. Fluorescence decay curve of the 1544 nm emission and its theoretical MC fit for (a) $(THF)_{14}Er_{10}S_6Se_{12}I_6$. The fitting parameters are $\tau_{rad} = 3.85$ ms, $R_{06} = 1.55$ nm, $R_{08} = R_{010} = 2.05$ nm, $R_0 = 2.05$ nm, and $L = 0.05$ nm. The fitting was done considering all the cooperative energy transfer (ET) upconversion processes and ESA from the pumping level $^4I_{11/2}$. (b) Exponential fit of the fluorescence decay in $(DME)_2Er(SC_6F_5)_3$.

Table 2. Comparison of the Fluorescence Lifetime and Phonon Frequencies of Some Reported Er-Containing Solid-State Materials

host	lifetime (ms)	phonon frequency (cm^{-1})	refs
sulfide	3.0	450−700	29
selenide	2.3	450−700	30
tellurite	4	450−700	4
germanate	6	900	4
ZBLA fluoride glass	10	500	4
fluorides, chlorides	10−30	200−400	4
yttrium aluminum garnet	8	400	4

difference in the crystal field strength experienced by the Er atom, which is determined by the nature of the ligand field and the symmetry of the molecule. The corresponding stimulated emission cross sections for Er10 and Er1 are 1.63×10^{-20} and 0.76×10^{-20} cm^2, respectively. These values are comparable to the cross-section of Er-doped LaF_3.[28] The emission intensity of Er10 is observed to be higher than that of Er1, primarily because of the higher volumetric concentration of Er ions.

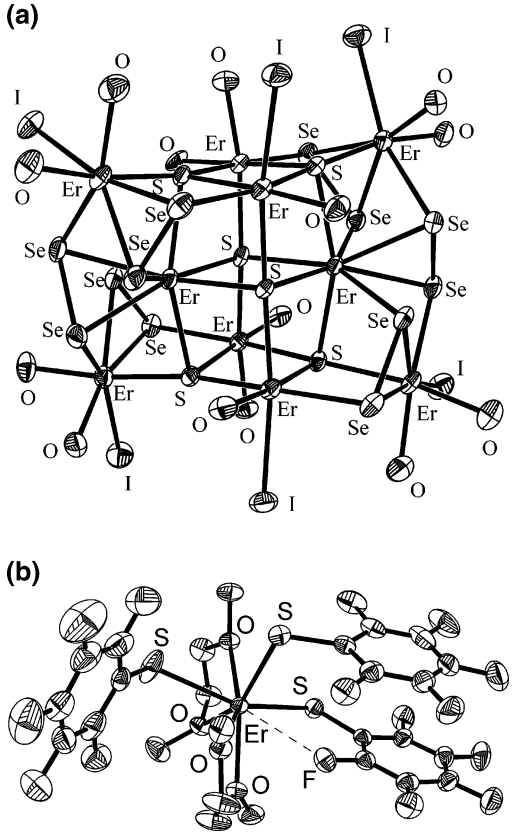

Figure 4. ORTEP diagrams for (a) $(THF)_{14}Er_{10}S_6Se_{12}I_6$, with the C and H atoms on the THF ligands (O) removed for clarity, and (b) $(DME)_2Er(SC_6F_5)_3$ with the labels for the C and F atoms removed for clarity.

Analysis of the energy transfer via MC simulation (eq 4) between the nearby Er ions in the Er10 cluster shows that there is strong multipolar interaction between them and the critical separation for the dipole−dipole interaction is estimated to be 1.55 nm. Because both the shortest and longest separation between two Er atoms in Er10 are both less than this distance, there is always a multipolar interaction between them to quench fluorescence emissions. This is further supported by the fluorescence decay characteristics shown in Figure 3a, which will now be discussed. In doing this simulation we considered the influence of the cooperative energy transfer upconversion (half-filled diamonds), excited-state absorption (ESA, open triangles), and the superposition of both (open circles) on the population decay of the $^4I_{13/2}$ level through the 1544 nm emission. The analysis shows the influence of both cooperative energy transfer upconversion and ESA quench are dominant in the 1544 nm emission because the experimental decay curve (closed squares) is fitted by this particular decay curve. Thus, the observed 22−25% reduction in quantum efficiency from 100% is attributed primarily to this nonradiative energy transfer processes.

Apart from multipolar energy transfer concentration quenching, the other major source of fluorescence quenching is normally from multiphonon relaxation due to the high-frequency vibrational bands of the ligand and absorption from nearby organic functional groups. In Er^{3+} compounds, one of the principle channels of multiphonon nonradiative decay is via $^4I_{11/2} \rightarrow {}^4I_{13/2}$ transitions, which is in the frequency region of 3700 cm^{-1}. This nonradiative channel can reduce the effective population density at the $^4I_{13/2}$ level and reduce

the fluorescence decay time and efficiency of the 1540 nm emission. Generally, chalcogenides, because of the low vibrational frequency (700 cm^{-1}), require more than five phonons to bridge the $^4I_{11/2} \leftrightarrow {}^4I_{13/2}$ gap, and the probability of such a higher order process is zero. Similarly, the population of the $^4I_{13/2}$ state during the $^4I_{13/2} \rightarrow {}^4I_{15/2}$ decay can be further lost by vibrational groups of frequency 6500 cm^{-1}. If Er^{3+} is directly attached to any of these vibrational groups or its harmonics, higher nonradiative loss can be expected, resulting in low quantum efficiency, as observed in all previously reported Er organic complexes reported so far. In most molecular Er complexes, the two main vibrational groups quenching the fluorescence efficiency of Er^{3+} are C−H and O−H. The second-order vibrational energy of C−H (2960 cm^{-1}) is resonant with the Er^{3+} first excited state (6500 cm^{-1}). Similarly, O−H is a potential quencher of Er luminescence, because its first vibrational overtone (3400 cm^{-1}) is strongly in resonance with the $^4I_{13/2} \rightarrow {}^4I_{15/2}$ transition (6500 cm^{-1}). In both Er1 and Er10, there are no OH functionalities, and the limited number of ligands with CH bonds are connected to the Ln through weak dative interactions, rather than covalent bonds between the metal cation and a hydrocarbon chain or hydroxide ion. In both complexes Ln ions are bound to heavy elements such as S, Se, I, and fluorinated thiolates, and because of the proximity of such heavy elements and fluorinated organic functionalities, high fluorescence quantum efficiency is achieved.

Conclusions

In conclusion, two new Er organometallic complexes of the formula $(THF)_{14}Er_{10}S_6Se_{12}I_6$ and $(DME)_2Er(SC_6F_5)_3$ were discovered, and these compounds show 75−78% quantum yield of emission at 1544 nm, which is comparable to inorganic hosts. This is the highest reported efficiency for organic complexes to date. The superior performance of this compound is interpreted as a result of the absence of high-frequency vibrational groups such as C−H and O−H in the core and the direct link of Er with heavy metals such as Se and I. This new organometallic cluster could be used as a potential candidate of 1544 nm emission in active optical devices where high quantum efficiency is a prerequisite for effective optical amplification.

Acknowledgment. We would like to acknowledge the support of NSF (CHE-0303075), New Jersey State Commission on Science and Technology, and USR Optonix for their generous support.

CM050770F